doi:10.2533/chimia.2025.25 Chimia 79 (2025) 25–28 © S. Menzi *et al.*

Extending Resonant Inelastic X-ray Scattering to Extreme Ultraviolet

Samuel Menzi[a], Fabio La Mattina[b], Francesco Barbato[b], Yunieski Arbelo Pena[b], Sven Augustin[a], Gregor Knopp[a], Marcello Coreno[c,d], Stefano Orlando[d], Monica de Simone[e], Paolo Miotti[f], Fabio Frassetto[f], Luca Poletto[f], Davide Bleiner[b,g], and Claudio Cirelli*[a,b]

Abstract: We present α-Al_2O_3 XAS, XES and RIXS measurements across the Al L_2/L_3 edges at about 79 eV excitation energy. In the emission spectra, we identify two fluorescence peaks, corresponding to electronic transitions into the 2*p* core hole from mixed states of Al 3*s* and Al 3*d* character, both mixed with O 2*p* orbitals. Even if the XAS spectrum shows more than one resonance, surprisingly only one clear RIXS signal with energy loss equal to 10.7 eV is present in the data. Nevertheless, this allows us to tentatively extract from the measured high-resolution data the linewidths for fluorescence and RIXS transitions, with the latter being almost a factor of two smaller than the former.

Keywords: EUV spectroscopy · Synchrotron experiments

1. Introduction

Resonant inelastic X-ray scattering (RIXS) is a powerful X-ray technique that allows for the investigation of the core and valence electronic structure of atoms, molecules and solids with selectivity of the scatterer's chemical state.[1] RIXS involves a second-order optical process, in which a core electron is excited by an X-ray photon and the excited state further decays by emitting an X-ray photon when a second electron fills the core hole. The technique is based on resonant excitation, achieved by tuning the incident photon energy close and across resonances, for instance in the proximity of an absorption edge. These excited core-hole resonance states decay into low energy excitations that are detected in the spectrum of the scattered light as inelastic (Raman) features. When the system is left in a final excited state, with local electronic excitation (inelastic scattering), the energy difference between the incoming and outgoing photons reveals the amount of energy transferred to the system.

RIXS comprises both absorption and emission processes because its intermediate state is at the same time equal to the final state of X-ray absorption (XAS) and to the initial state of X-ray fluorescence (emission, XES). Consequently, the available information is much richer than that one given by the individual first-order XAS or XES processes: both unoccupied and occupied states are probed simultaneously within a single process. Furthermore, since it is a photon-in / photon-out technique, it can be applied to solid targets in the presence of applied electric and magnetic fields, both to metals and insulators.

The signal levels of such second order process are much weaker than the first-order ones, mainly because of the low efficiency of the X-ray emission. Nevertheless, in the hard X-ray energy range, where the cross sections for the X-ray emission process are relatively high, it has been shown that techniques like high-energy resolution fluorescence detected (HERFD)[2,3] or other methods based on the same Kramer–Heisenberg formalism as RIXS,[4] allow to obtain an absorption spectrum with a higher energy resolution than standard XAS.

Nevertheless, since RIXS considers two-photons transitions, it can also allow the study of intraband excitations between orbitals of the same symmetry, a class of processes forbidden by the electric dipole selection rules and therefore only partially accessible by other techniques such as optical absorption spectroscopy. Among these excitations, the most interesting are the ones involving *dd* transitions on the cation site in a compound with a 3*d* transition metal center[5] and low energy transitions in low-Z elements.

To-date, most of the studies in transition metal compounds have been performed with incident photon energies in the soft X-ray range, aiming at $L_{2,3}$ edges, while RIXS data at $M_{2,3}$ edges, lying in the extreme ultraviolet (EUV) energy range, are much less common.[6] This is mainly due to several experimental challenges, among which are the presence of non-radiative competitive processes and the amplitude of elastic scattering that generally hinders the observation of inelastic features at very small transferred energy ($E \sim 0.5$ eV).[7]

On the other hand, the extension of RIXS to EUV entails the advantages of a higher energy resolution being achievable and a lower energy transfer to the system, resulting in fewer simultaneous excited collective modes. More recently it has been shown that using high-flux beamlines in combination with high-acceptance spectrometers, $M_{2,3}$-RIXS experiments are possible with good signal-to-noise ratios.[8]

Here we present the first results based on the measurements of EUV RIXS performed at the Al L-edges in aluminum oxide.

Due to its industrial importance, α-Al_2O_3 has been heavily investigated in the past with X-ray spectroscopy. The electronic structure was explored with X-ray based techniques such as XAS in total fluorescence yield (TFY) and electron yield (TEY), XES, electron energy loss spectroscopy.[9,10]

*Correspondence: Dr. C. Cirelli, E-mail: claudio.cirelli@psi.ch
[a]Laboratory for Synchrotron Radiation and Femtochemistry, Center for Photon Science, Paul Scherrer Institut (PSI), CH-5232 Villigen, Switzerland; [b]Swiss Federal Laboratories for Materials Science and Technology (Empa), Überlandstrasse 129, CH 8600 Dübendorf; [c]ELETTRA - Sincrotrone Trieste, Basovizza Area Science Park, S. S. 14 – km 163.5, I-34149, Basovizza (TS), Italy; [d]CNR – Istituto di Struttura della Materia (ISM), in Basovizza Area Science Park, I-34149, Trieste, Italy; [e]CNR - Istituto Officina dei Materiali (IOM), S. S. 14 - km 163.5, I-34149, Trieste, Italy; [f]CNR – Istituto di Fotonica e Nanotecnologie (IFN), via Trasea 7, I-35131 Padova, Italy; [g]University of Zurich, Winterthurerstrasse 190, CH-8053, Zurich

Our data complements these studies, presenting the first RIXS data measured upon excitation in the EUV energy range. We tentatively identify the involved states contributing to the RIXS signals and interpret the observed signal with the help of a multi-Voigt global fitting procedure. This allows us to extract excited state lifetimes of valence band energy states involved in the RIXS process. As already mentioned before, these states are generally not accessible by direct absorption processes due to selection rules.

We show that our results provide a better insight into the aluminum oxide electronic structure.

2. Experiments

The sample was an α-Al_2O_3 crystal cut along the (1, 0, -1, 2) direction. The measurements were performed at the GASPHASE beamline[11] of the Elettra synchrotron, using linearly polarized EUV synchrotron radiation.

2.1 *XAS Measurements*

Knowledge of the absorption spectrum is a prerequisite for performing RIXS experiments since the excitation energy has to be tuned close to an absorption peak.

We tested two independent methods to measure the absorption spectrum of aluminum oxide in the proximity of the Al L-edges: (i) reflectivity and (ii) TEY.

As shown in Fig. 1a, for the reflectivity measurement, the synchrotron beam reflected by the sample, positioned at 20 degrees grazing incidence with respect to the incoming EUV beam, was collected by a photodiode. This geometry is particularly advantageous because an XAS in reflectivity can be quickly measured without changing the experimental setup optimized for the long-lasting RIXS/XES measurements. This allowed us to periodically monitor the shape of the absorption spectrum and estimate the sample radiation damage, which can be particularly relevant for samples exposed to soft X-ray and EUV radiation.[12]

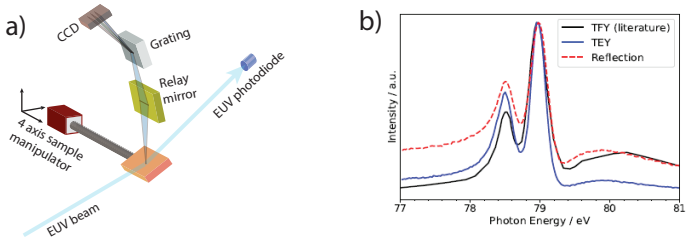

Fig. 1. a) Experimental setup adopted for simultaneous emission (for RIXS) and reflection (for XAS) measurements. The sample was oriented to 20 degrees with respect to the incident beam. b) Comparison between absorption spectra measured at the Al $L_{2,3}$ edges for α-Al_2O_3 sample. The red dash line shows the spectrum recorded in reflection, while the blue solid line the one measured in total electron yield. A reference spectrum[16] collected in total fluorescence yield (black solid line) is also shown. The TFY spectrum was shifted by +30 meV for best agreement.

At the beginning of the experiment, we verified that the TEY and reflectivity methods deliver the same information, Fig. 1b. The conventional method of measuring the absorption in the TEY mode consists in collecting the photoelectrons with a high current channeltron detector. In our setup (Fig. 1a) the detector was placed over the sample surface in the same position as where the EUV spectrometer[13] was used for the RIXS measurements.

It has already been demonstrated that the sample response measured in reflection is connected *via* the Kramers–Kronig relation to the absorption spectrum.[14,15] Indeed, the resulting spectra are compared in Fig. 1b. They show good qualitative agreement, even though being intrinsically different spectra. Both XAS spectra closely match the literature data.[15,16]

2.2 *RIXS Measurements in the EUV*

After collecting the absorption TEY spectrum, the channeltron detector was replaced with the EUV spectrometer and RIXS data were measured scanning the incident photon energy across the aluminium $L_{2,3}$ absorption edges. Fig. 2a shows the resulting RIXS plane.

In Fig. 2 one can distinguish two distinct X-ray fluorescence peaks (brown), at constant emission energies of 63.3 and 67.7 eV. RIXS peaks have an emission energy that linearly disperses with varying incident energy. As a guide for the eye, two lines representing constant emission energy and one line representing a linear trend with a slope of 1 are drawn on the RIXS plane, Fig. 2b. The TEY absorption spectrum shown in Fig. 1b is plotted in the inset and can be used as a reference for the excitation energy.

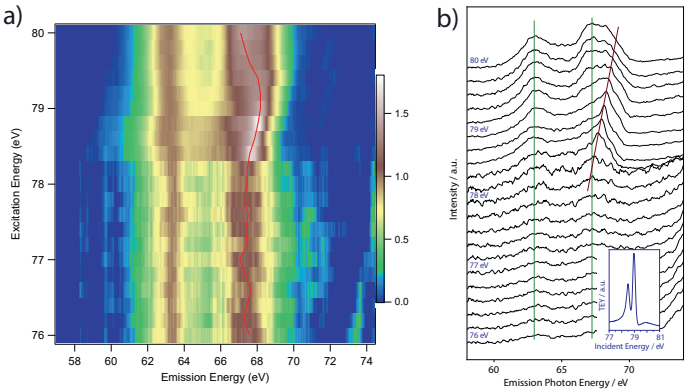

Fig. 2. a) RIXS plane measured across the $L_{2,3}$ edges in α-Al_2O_3 with photon energy ranging from 76 to 80 eV in steps of 0.2 eV. Note that each XES spectrum is normalized to its maximum value just for clarity. The red line marks the position of the maximum in each spectrum recorded for a different excitation energy. b) Not normalized individual XES spectra extracted from the 2D RIXS plane at different excitation energies. The latter can be identified in the XANES spectrum shown in the inset. The green vertical lines represent the positions of the constant emission energies 63.3 and 67.7 eV, while the red line follows the inelastic signal (RIXS) with a constant transferred energy of 10.7 eV.

The most prominent RIXS signal emerges at an emission energy of about 68 eV for excitation energies around 78.8 eV, *i.e.* resonant with the second absorption peak (L_2 edge). For this feature the constant transferred energy is 10.7 eV. The observation of electronic transitions with lower transferred energy are unfortunately hindered by the presence of the intense elastic scattering peak.

With the support of the XAS data (Fig. 1b), it is possible to identify the transitions involved in the RIXS signal detected at 10.7 eV. The XAS consists of two sharp peaks at 78.5 and 78.9 eV and one broad feature at about 80 eV. The sharp peaks arise due to excitation of the Al 2*p* electrons into states with 3*s* character. This $2p^6 3s^0$ - $2p^5 3s^1$ transition yields a spin-orbit coupled $2p^5$ configuration, giving rise to two excitation edges for $J = l+s = 3/2$ and $J = l–s = 1/2$.

The transition at lower energy populates the $J = 3/2$ manifold and the transition at higher energy the $J = 1/2$ manifold. The intensity ratio of the two peaks is approximately 2:1, reflecting the multiplicities (2J+1) of the states. The Al edges are denoted L_3-edge at lower energy and L_2-edge at higher energy and have a spin-orbit splitting value of ~0.5 eV, which is in agreement with the energy difference measured between the two sharp peaks in the XAS.

The XES spectrum (Fig. 2) shows two fluorescence peaks, corresponding to an electronic transition into the 2*p* core hole from mixed states of Al 3*s* and Al 3*d* character, both mixed with O 2*p* orbitals.

The detected RIXS signal has an energy loss of 10.7 eV. Since this RIXS process involves the Al 2*p*-3*s* transition at 78.9 eV, it has to be coherently coupled with a XES signal at 68.2 eV. In the experimental data, the emission line is at 67.7 eV, *i.e.* 0.5 eV off with respect to the expected value.

2.3 *Fitting of a Multi-Voigt Model*

With the goal of extracting the widths, areas and positions of the peaks in the RIXS plane, a multi-Voigt global peak model was built and used to fit to the data of Fig. 2. We used a sum of Lorentzian or Voigt profiles, which are known to be able to describe reasonably well both the absorption (TFY) and emission spectra,[16] accounting also for the instrumental energy resolution.

While in the experimental data in Fig. 2 only one RIXS peak and at least two fluorescence peaks are clearly apparent, the number of unresolved peaks may likely be larger. The number of peaks required to represent the data within the model was found iteratively. First, the number of fluorescence peaks in the RIXS plane was guessed and to each peak a parameter was attributed for its position along the emitted photon energy (in the following denoted $\hbar\omega_2$) and a parameter for its Lorentzian width component of the Voigt profile, as well as three parameters (one for each absorption peak) for the amplitude along the excitation photon energy (labeled as $\hbar\omega_1$) axis.

The number of fluorescence peaks used in the model was increased until the best agreement with the data was achieved.

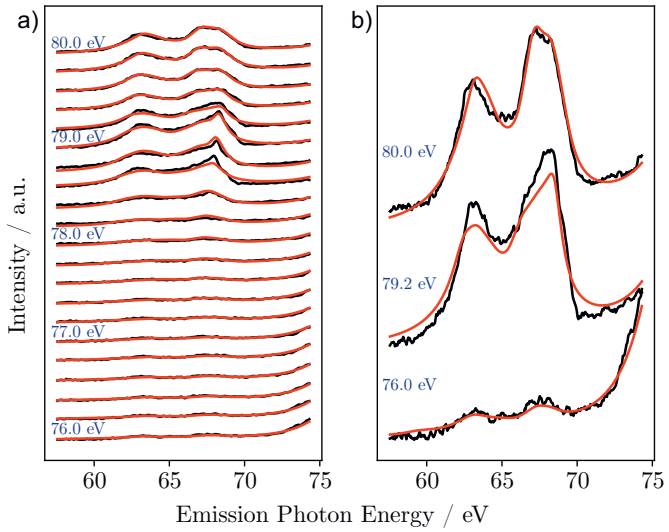

Fig. 3. Comparison of the experimental data (black) to the fitted model (red). a) All spectra are shown, b) Spectra at 76 eV, 79.2eV, and 80 eV are magnified for comparison.

A model based on only two fluorescence peaks is not able to describe the measured signals, but satisfactory agreement is found when up to six peaks are considered. The result of the global fitting procedure is shown in Fig. 3.

Before discussing the outcome of the fit results shown in Fig. 3, we first elucidate some aspects of the fitting model, with the help of Fig. 4. Here we show the curves calculated using the parameters returned by the fit procedure for the most intense fluorescence (shown in green) and RIXS (shown in orange) peaks. These transitions are the ones originating from an excitation resonant with the most intense XAS feature, at 78.9 eV.

The RIXS plane formed by these two transitions is shown on the left panel of Fig. 4, where one can see the asymmetric intensity shape due to the different nature of the RIXS and fluorescence processes. In fact, while the energy position of the fluorescence peak stays at constant emitted photon energy $\hbar\omega_2$ for different excitation photon energy $\hbar\omega_1$, the RIXS energy peak position disperses within the plane.

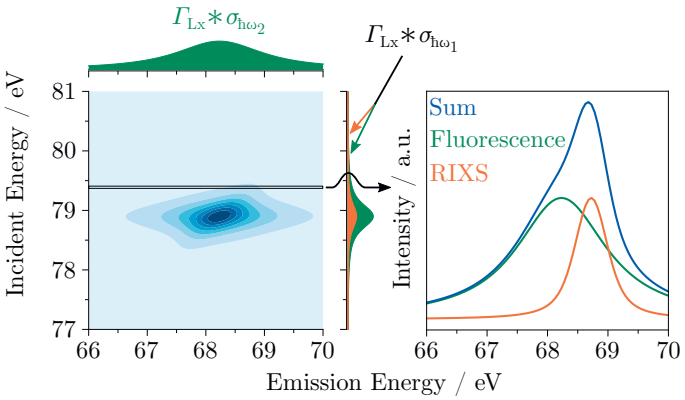

Fig. 4. The left panel shows an exemplary RIXS plane, mapped with a color gradient going from white (zero intensity) to dark blue (maximum intensity); the horizontal energy axis is the emission energy. The peaks in the 2D spectra are projected onto the two axes, resulting in the Voigt profiles on the sides. The green distribution represents the fluorescence peak while the orange one represents the RIXS peak. On the right, lineouts for the fluorescence and RIXS contributions and their sum are shown for an incident energy of 79.4 eV. Note that in this example the instrumental resolution $\hbar\omega_2$ is larger than $\hbar\omega_1$.

Both distributions peak when the incident energy equals the absorption resonance at 78.9 eV, as indicated by the green and orange projections shown on the right side of the RIXS plane.

A projection onto the incident energy axis yields the partial fluorescence yield (PFY) absorption spectrum with the shape of a Voigt profile composed by the convolution of a Lorentzian function, whose broadening is due to the core-hole lifetime Γ_{Lx}, and a Gaussian function, with the broadening purely due to the instrumental resolution $\hbar\omega_1$. Note that the projected RIXS peak and the projected fluorescence peak have the same width and only vary in their intensity.

On the other hand, a projection of the fluorescence peak onto the emission energy axis returns the non-resonant XES spectrum with the Voigt broadening corresponding to Γ_{Lx} and $\sigma_{\hbar\omega 2}$.

The right panel of Fig. 4 shows the individual contributions and the sum of only the most intense fluorescence and RIXS transitions for an incident energy $\hbar\omega_1$ = 79.4 eV. The results of the global fit are shown on the left of Fig. 3. The energy positions of the fluorescence peaks E_{fluo} were left as fit parameters, while the energy position of the RIXS peaks were calculated by the energy conservation equation:

$$E_{RIXS} = \hbar\omega_1 - E_{abs} + E_{fluo} \quad (1)$$

For any incident energy $\hbar\omega_1$ it is possible to solve this equation for E_{RIXS} because the corresponding absorption energy E_{abs} is known from the XAS. The three absorption peaks observed in the XAS combined with six fluorescence peaks can give rise to many RIXS peaks, in the case where the final state of the absorption transition is the same as the initial state in the fluorescence transition.

As already indicated, the Voigt peak widths along the $\hbar\omega_2$ axis are fitted with one parameter per peak representing the lifetime

broadening, a quantity assumed to be constant for all the spectra. A single parameter representing the instrumental resolution along the $\hbar\omega_2$ axis can be estimated from the measurements of the elastic peak widths performed for the energy calibration of the detector. This yields a Gaussian width of 0.15 eV, which is imposed as a fix parameter to the fitting routine.

The measured signals are represented by Voigt profiles not only along the $\hbar\omega_2$ axis but also along the $\hbar\omega_1$ axis, with three independent Lorentzian width parameters convoluted with a single Gaussian width parameter, representing the instrumental resolution along the $\hbar\omega_1$ axis.

Each RIXS peak along the $\hbar\omega_2$ axis is also fitted with individual Lorentzian width parameters. Since the valence level hole is located at a much lower binding energy than the L-edge core hole, it is expected that the lifetime broadening of the RIXS transition will be smaller than the corresponding fluorescence one.

The most intense RIXS transition is the one involving absorption at the Al L_2-edge (at 78.9 eV). The spectral broadening of the most intense RIXS transition along the emitted energy axis $\hbar\omega_2$ was found to be 0.37 eV, narrower by about a factor of two than the corresponding fluorescence line.

While the model shows satisfactory agreement with the experiment, the results have to be carefully interpreted due to the large number of fit parameters involved. Additional *ab initio* calculations of the RIXS plane would allow constraints on the fit parameters to be set, such as the number of possible RIXS peaks, potentially allowing the extraction of more accurate information.

Nevertheless, the fit procedure was able to provide a tentative insight into the linewidth of the most prominent observed spectral features. The linewidths Γ_{L2} and Γ_{L3} estimated from the fit for the fluorescence lines at emission energies $\hbar\omega_2$ equal to 63.3 and 67.7 eV are 1.94 and 0.8 eV, respectively.

The narrower spectral broadening of the RIXS peak in comparison to the fluorescence peak is a consequence of the different states responsible for the line broadening. In the case of XES, the broadening depends on the lifetime of the initial state, while in RIXS the broadening depends on the final state.

3. Conclusions

We have shown the first measurements of RIXS across the $L_{2,3}$ edges of alpha phase aluminum oxide in the EUV.

By inspecting the absorption spectrum, we tentatively assign the transitions involved in the process.

A fit of the measured spectra in the RIXS plane with a multi-Voigt model returns an estimate of the spectral broadening, and therefore the core (from the XES line) and valence (from the RIXS line) hole lifetimes.

These results show the promising perspectives of extending RIXS in the EUV range. The spectra allow the possibility to determine both long and short core hole lifetimes at the same resonance edge.

Furthermore, for heavier elements than aluminium, which have resonances accessible both in the EUV and soft X-ray range (like transition metals M and L edges), EUV RIXS spectra may complement the soft X-ray RIXS information on the electronic structure configuration of the system under study.

Acknowledgements

Financial support from the Swiss National Science Foundation (SNSF) through grant No. 200021_169454 is gratefully acknowledged.

Author Contributions

C. C. and D. B. conceived the experiment, S. M., F. B., Y. A. P., G. K., F. L., M. C., S. O., M. D., L. P., P. M., F. F. and C. C. participated in collecting the data, S. M., S. A. developed the data analysis. All authors participated in interpreting the results and writing the manuscript.

Received: October 30, 2024

[1] L. J. P. Ament, M. van Veenendaal, T. P. Devereaux, J. P. Hill, *Rev. Mod. Phys*. **2011**, *83*, 63, https://doi.org/10.1103/RevModPhys.83.705.
[2] P. Glatzel, T.-C. Weng, K. Kvashnina, J. Swarbrick, M. Sikora, E. Gallo, N. Smolentsev, R. Alonso Mori, *J. Electron Spectrosc. Relat. Phenom.* **2013**, *9*, 17, https://doi.org/10.1016/j.elspec.2012.09.004.
[3] F. M. F. de Groot, M. H. Krisch, J. Vogel, *Phys. Rev. B* **2002**, *66*, 195112, https://doi.org/10.1103/PhysRevB.66.195112.
[4] M. Rovezzi, P. Glatzel, *Semicond. Sci. Technol*. **2014**, *20*, 2, http://doi.org/10.1088/0268-1242/29/2/023002.
[5] S. M. Butorin, J.-H. Guo, M. Magnuson, P. Kuiper, J. Nordgren, *Phys. Rev. B* **1996**, *54*, 4405, http://doi.org/10.1103/PhysRevB.54.4405.
[6] P. Kuiper, J.-H. Guo, C. Såthe, L.-C. Duda, J. Nordgren, J. J. M. Pothuizen, F. M. F. de Groot, G. A. Sawatzky, *Phys. Rev. Lett.* **1998**, *80*, 5204, http://doi.org/10.1103/PhysRevLett.80.5204.
[7] L. A. Wray, S.-W. Huang, I. Jarrige, K. Ikeuchi, K. Ishii, J. Li, Z. Q. Qiu, Z. Hussain, Y.-D. Chuang, *Front. Phys*. **2015**, *3*, http://doi.org/10.3389/fphy.2015.00032.
[8] S. G. Chiuzbăian, G. Ghiringhelli, C. Dallera, M. Grioni, P. Amann, X. Wang, L. Braicovich, L. Patthey, *Phys. Rev. Lett*. **2005**, *95*, 197402, http://doi.org/10.1103/PhysRevLett.95.197402.
[9] R. H. French, *J. Am. Ceram. Soc*. **1990**, *73*, 477, http://doi.org/10.1111/j.1151-2916.1990.tb06541.x.
[10] A. Balzarotti, A. Bianconi, *Phys. Status Solidi (b)* **1976**, *76*, 689, http://doi.org/10.1002/pssb.2220760230.
[11] M. Alagia, L. Avaldi, M. Coreno, R. Camilloni, C. Furlani, K. C. Prince, R. Richter, M. De Simone, G. Stefani, S. Stranges, *Synchrotron Radiat. News* **2003**, *16*, 19, http://doi.org/10.1080/08940880308603010.
[12] M. Kubin, J. Kern, M. Guo, E. Källman, R. Mitzner, V. K. Yachandra, M. Lundberg, J. Yano, P. Wernet, *Phys. Chem. Chem. Phys.* **2018**, *20*, 16817, http://doi.org/10.1039/C8CP03094D.
[13] L. Poletto, F. Frassetto, P. Miotti, A. Di Cicco, P. Finetti, C. Grazioli, F. Iesari, A. Kivimäki, S. Stagira, M. Coreno, *Rev. Sci. Instrum.* **2014**, *85*, 103112, http://doi.org/10.1063/1.4898315.
[14] D. Alders, T. Hibma, G. A. Sawatzky, K. C. Cheung, G. E. van Dorssen, M. D. Roper, H. A. Padmore, G. van der Laan, J. Vogel, M. Sacchi, *J. App. Phys*. **1997**, *82*, 3120, http://doi.org/10.1063/1.366153.
[15] W. L. O'Brien, J. Jia, Q.-Y. Dong, T. A. Callcott, D. R. Mueller, D. L. Ederer, C.-C. Kao, *Phys. Rev. B* **1993**, *47*, 15482, http://doi.org/10.1103/PhysRevB.47.15482.
[16] C. Weigel, G. Calas, L. Cormier, L. Galoisy, G. S. Henderson, *J. Phys.: Condens. Matter*. **2008**, *20*, 135219, http://doi.org/10.1088/0953-8984/20/13/135219.